Available online at www.sciencedirect.com
ScienceDirect
Colloids and Surfaces B: Biointerfaces 54 (2007) 127–135
COLLOIDS AND SURFACES B
www.elsevier.com/locate/colsurfb

Glyco-acrylate copolymers for bilayer tethering on benzophenone-modified substrates

Lisa Y. Hwang [a], Heide Götz [b], Craig J. Hawker [c], Curtis W. Frank [a,*]

[a] *Department of Chemical Engineering, Stanford University, 381 North-South Mall, Stanford, CA 94305-5025, United States*
[b] *European Patent Office, Bayerstrasse 34, 80335 München, Germany*
[c] *Department of Chemistry and Biochemistry, University of California Santa Barbara, Santa Barbara, CA 93106-9510, United States*

Received 13 June 2006; received in revised form 5 August 2006; accepted 8 August 2006
Available online 22 August 2006

Abstract

Model biological membranes are becoming increasingly important for studying fundamental biophysical phenomena and developing membrane-based devices. To address the anticipated problem of non-physiological interactions between membrane proteins and substrates seen in "solid-supported lipid bilayers" that are formed directly on hydrophilic substrates, we have developed a polymer-tethered lipid bilayer system based on a random copolymer with multiple lipid analogue anchors and a glyco-acrylate backbone. This system is targeted at applications that, most importantly, require stability and robustness since each copolymer has multiple lipid analogues that insert into the bilayer. We have combined this copolymer with a flexible photochemical coupling scheme that covalently attaches the copolymer to the substrate. The Langmuir isotherms of mixed copolymer/free lipid monolayers measured at the air–water interface indicate that the alkyl chains of the copolymer lipid analogues and the free lipids dominate the film behavior. In addition, no significant phase transitions are seen in the isotherms, while hysteresis experiments confirm that no irreversible states are formed during the monolayer compression. Isobaric creep experiments at the air–water interface and AFM experiments of the transferred monolayer are used to guide processing parameters for creating a fluid, homogeneous bilayer. Bilayer homogeneity and fluidity are monitored using fluorescence microscopy. Continuous bilayers with lateral diffusion coefficients of 0.6 $\mu m^2/s$ for both leaflets of the bilayer are observed for a 5% copolymer system.

Keywords: Planar lipid bilayers; Biomimetic membrane; Polymer-tethered bilayers

1. Introduction

The high complexity of biological membranes and their interactions with various cellular systems make direct investigations extremely difficult. Therefore, model membranes have become essential for fundamental biophysical research of membrane-related phenomena. Membrane-based devices have also been developed as the understanding of biomembranes has grown and potential applications have emerged. One of the most promising model membrane designs uses a planar substrate on which to assemble the membrane [1]. For over 20 years, the most commonly used model system has been a phospholipid bilayer deposited onto a solid substrate [2], thus creating a "solid-supported lipid bilayer". Several studies using solid-supported lipid bilayers have concentrated solely on understanding the properties of the lipid bilayer, including studies of lipid assemblies on surfaces [3–6], lipid bilayer dynamics [7,8], and lipid bilayer electrochemical properties [9,10]. Other studies have incorporated select membrane proteins to investigate immune responses and cell adhesion [11–13], ligand–receptor interactions [14,15], and lipid–protein interactions [16]. Additional work has focused on the development of membrane-based devices such as biosensors and microseparation devices [17,18].

However, solid-supported lipid bilayers have some fundamental limitations due to the proximity of the bilayer and the substrate. The thin (1–2 nm) lubricating layer of water that separates the bilayer from the substrate [19–21] is sufficient to retain long-range lipid mobility [22–24]. However, when bilayers containing transmembrane proteins are deposited onto the substrate, the substrate can interact with the proteins, leading to non-specific adsorption of the protein to the substrate. This has

* Corresponding author. Tel.: +1 650 723 4573; fax: +1 650 723 9780.
E-mail address: curt.frank@stanford.edu (C.W. Frank).

0927-7765/$ – see front matter © 2006 Elsevier B.V. All rights reserved.
doi:10.1016/j.colsurfb.2006.08.010

been shown to inhibit protein lateral mobility [25,26] and may lead to denaturation and loss of functionality.

One strategy that has been developed to overcome these limitations is to insert a hydrophilic polymer layer between the substrate and the bilayer. Ideally, this polymer layer separates the bilayer from the substrate while also providing a lubricating surface for the bilayer that may assist in bilayer healing. Many variations of this strategy have emerged. One variation uses a polymer cushion that is not covalently attached to the bilayer, but rather relies on bilayer–polymer interactions to hold the assembly together [27–30]. However, designing mechanically and thermodynamically stable polymer-cushioned lipid bilayers can be difficult since the wetting conditions of the substrate–polymer interface, substrate–bilayer interface, and polymer–bilayer interface must be carefully controlled [31,32]. This leads to reduced long-term stability, especially if the proteins of interest transport molecules such as ions, which could disturb the delicate interactions that hold the structure together.

Building upon the idea of incorporating a polymer to create separation between the bilayer and substrate, another successful model membrane strategy has been to insert polymers with covalently attached lipid analogues that integrate into the lower leaflet of the lipid bilayer ("lipopolymers") [33,34]. Unlike the cushioned model membranes that rely on interactions such as electrostatic attraction to stabilize the various layers, these tethered lipid bilayers have lipid analogue anchor groups that stabilize the polymer–bilayer interface. They are also covalently linked to the substrate to provide additional robustness. Several methods can be used to create this type of model membrane including self-assembly [35] and Langmuir–Blodgett (LB) techniques [36–39]. Although LB techniques can be significantly more time-consuming than self-assembly, they offer tremendous control over the organization of the film. In addition, the use of LB transfer to deposit the monolayer substantially broadens the range of substrates that can be used as the base for this model membrane in terms of both substrate chemistry and topography. Several other design aspects of these polymer-tethered lipid bilayers must also be carefully considered including the chemistry of the polymer, the method of covalent tethering, and the degree of tethering. These options allow for the controlled variation of several crucial assembly parameters including the polymer–substrate and polymer–bilayer interactions, the polymer chain conformation, and the area per phospholipid in the bilayer, all of which will dictate the physical properties of the final bilayer.

In this study, we present a random copolymer-tethered lipid bilayer system that has been developed to target applications that require stability and robustness. These random copolymers have multiple lipid analogues along the polymer backbone that insert into the bilayer and that may increase the robustness and stability of the structure. A random copolymer-tethered monolayer was first created using LB techniques, followed by vesicle fusion to deposit the distal leaflet of the bilayer. The copolymer chosen for this study has a glyco-acrylate backbone that approximates the native cellular environment of a glycocalix, which could potentially enhance the biocompatibility and performance of devices derived from this polymer system. The copolymer also carries monomers with bis-substituted C_{18} alkyl chains as lipid analogues that insert into the bilayer. A well-defined random copolymer lipopolymer consisting of 85% D-glucose-2-propenoate (glyco-monomers), 15% *N*,*N*-di(octadecyl)acrylamide (lipid-monomers, "DODA"), and a terminal 4′-*N*,*N*-di(octadecyl)aminomethyl phenylethoxy ("CO15") was previously synthesized from a living free-radical polymerization [40]. L-α-Phosphatidylcholine from egg (egg-PC) was used as the free lipid in the monolayer and vesicles because of its existence as a liquid phase monolayer over a wide range of temperatures. Mixtures of the copolymer and free lipid were organized at the air–water interface, and then deposited onto solid substrates using LB transfer. These substrates were chemically modified prior to transfer with a silane-benzophenone coupling agent. A light-induced reaction between the benzophenone groups and C–H bonds present in the copolymer was used to covalently attach the copolymer to the substrate. This coupling scheme was chosen because benzophenone moieties are able to covalently bond to C–H bonds of most molecules quickly, efficiently, and in a number of chemical environments [41]. The bilayer was completed using vesicle fusion with small unilamellar vesicles of egg-PC. This study details the properties of the monolayer at the air–water interface, the transferred monolayer in air, and the final bilayer in aqueous environment. Conditions that produce homogeneous, fluid bilayers are explored.

2. Experimental section

2.1. Materials

L-α-Phosphatidylcholine from egg (egg-PC) was purchased from Avanti Polar Lipids (Alabaster, AL). *N*-(Texas Red sulfonyl)-1,2-dihexadecanoyl-*sn*-glycero-3-phosphoethanolamine, triethylammonium salt (Texas Red-PE) was purchased from Molecular Probes (Eugene, OR). Random copolymers consisting of D-glucose-2-propenoate, *N*,*N*-di(octadecyl)acrylamide, and a terminal 4′-*N*,*N*-di(octadecyl)aminomethyl phenylethoxy ("CO15") were previously synthesized using a nitroxide-mediated living free-radical polymerization (M_n = 14,000; PDI = 1.17) [40]. The chemical structure of CO15 is shown in Fig. 1. 4-(3′-Chlorodimethylsilyl)propyloxybenzophenone, the photocoupling agent, was synthesized following a procedure described pre-

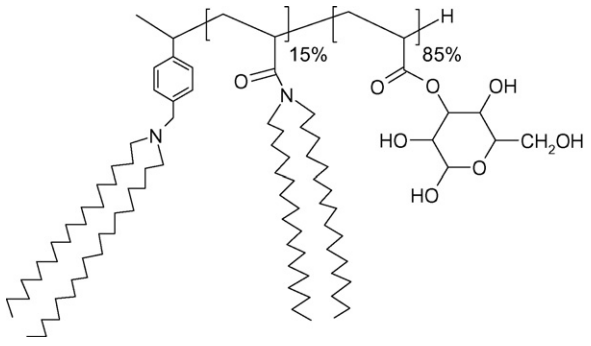

Fig. 1. Structure of random D-glucose-2-propenoate/*N*,*N*-di(octadecyl) acrylamide copolymer ("CO15").

viously [42]. Seven times detergent was purchased from ICN Biomedicals Inc. (Aurora, OH). Purified deionized water with a resistivity of 18.2 MΩ cm was obtained using the Millipore Milli-Q system (Billerica, MA).

2.2. Substrate cleaning

Glass cover slip substrates were used for fluorescence experiments and silicon wafer substrates were used for AFM experiments. (It should be noted that any substrate that can be functionalized with the benzophenone coupling agent could be used. We are using silicon oxide substrates as representative substrates.) The glass cover slips were heated to ∼85 °C in 7× detergent diluted to 1:4 v:v in Millipore water for at least 15 min, followed by extensive rinsing in deionized (DI) water. The cover slips were dried under a N_2 stream and then baked in air at 400 °C for 4 h. The silicon substrates were rinsed with ethanol, dried under a N_2 stream, and oxygen-plasma cleaned for 5 min at 75 W with a March Plasmod Plasma Etcher (March Instruments Inc., Concord, CA).

2.3. Substrate modification

The freshly cleaned substrates were placed in an immobilization solution of 1.3 g/L of 4-(3′-chlorodimethylsilyl)-propyloxybenzophenone prepared in dry toluene. Triethylamine, which acts as a catalyst and acid scavenger, was added to the solution at a ratio of 2 mL triethylamine for every 21 mL of immobilization solution. This immobilization step was carried out under N_2 at room temperature for 4–5 h. The substrates were then rinsed extensively with toluene and dried under a N_2 stream. A schematic of this immobilization step is shown in the first half of Fig. 2.

2.4. Film balance measurements and Langmuir–Blodgett transfer

All surface pressure–area isotherms and transfers were carried out in a 50 cm × 15 cm symmetric-compression KSV 5000 Langmuir–Blodgett trough (Helsinki, Finland). The subphase was Millipore water held at a constant temperature of 26.0 ± 0.2 °C. Stock solutions of CO15 copolymer were made in 19:1 v:v chloroform: methanol due to the poor solubility of CO15 in pure chloroform. Mixtures of CO15/egg-PC were prepared at various mol% CO15. Here, the mol% refers to the lipid-like DODA moieties on the copolymer rather than simply the mol% of CO15 since each copolymer contains multiple DODA moieties. For example, the label "5 mol% CO15" indicates a solution that contains 5 mol% DODA moieties, which are attached to a CO15 copolymer (actual mol% of the CO15 copolymer is less than 1). These spreading solutions of CO15/egg-PC mixtures were prepared at 0.5–2.0 mg lipid-like group (DODA and egg-PC)/mL. For experiments in which the proximal leaflet was labeled with Texas Red-PE, 0.6 mol% Texas Red-PE was added to the mixed CO15/lipid solution. The molar ratio of CO15 to lipid was kept as stated, while the lipid content included both egg-PC and Texas Red-PE. For example, the fluorescently labeled 5% CO15 solution contained 94.4 mol% egg-PC and 0.6 mol% Texas Red-PE to make up the remaining 95 mol% free lipid. The barrier compression rate in the experiments was set at a forward and backward speed of 10 mm/min. For LB transfers, a wait time of at least 25 min was used once the monolayers were compressed to the target surface pressure prior to initiating the transfer. During this wait time, the barriers were allowed to move at a forward and backward speed of 10 mm/min in order to maintain the target surface pressure. (The barrier compensation required to maintain the target surface pressure is dependent on the monolayer composition and target surface pressure as discussed in Section 3 and Fig. 6.) LB transfers were carried out at a transfer speed of 0.5 mm/min and a constant surface pressure of 25 mN/m (unless specifically stated otherwise).

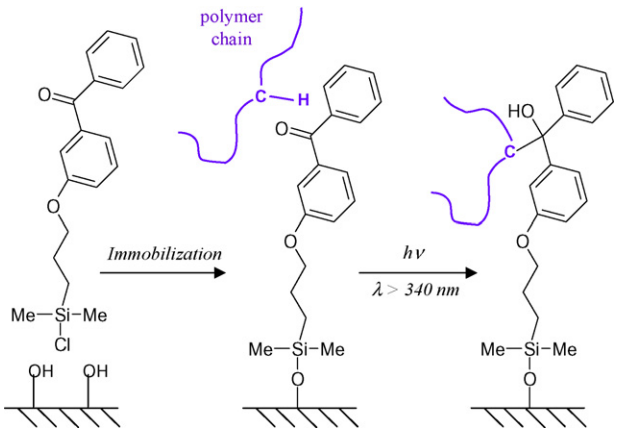

Fig. 2. Benzophenone surface immobilization and subsequent covalent attachment of the lipopolymer via UV illumination.

2.5. Photochemical attachment

Immediately following the LB transfer, the substrates were illuminated with UV light (λ > 340 nm) from an Oriel Instruments mercury UV lamp (Stratford, CT) for 5 min under ambient conditions. A schematic of this attachment is shown in the latter half of Fig. 2.

2.6. Vesicle preparation and bilayer formation

Small unilamellar vesicles (SUVs) were prepared using the standard extrusion method, as described elsewhere [43,44]. Briefly, chloroform was evaporated from egg-PC, with or without Texas Red-PE, by a stream of nitrogen. After being dessicated under vacuum for at least 1.5 h, the lipids were hydrated in Millipore water at 5 mg/mL. The resulting suspension was extruded 31 times through a polycarbonate membrane of 100 nm pore diameter using a Mini-Extruder (Avanti Polar Lipids, Alabaster, AL). Immediately prior to performing vesicle fusion to form the bilayer, equal volumes of vesicle solution and standard buffer (10 mM Tris, 100 mM NaCl adjusted to pH 8 using NaOH) were mixed to create a final vesicle fusion solution of 2.5 mg/mL. A small droplet of this solution was placed in a clean Petri dish. The substrate with LB transferred monolayer

was placed face down on the droplet, and the vesicle solution spread to cover the entire face of the substrate. The substrate was allowed to sit on top of the droplet for 1 h to ensure complete vesicle fusion.

2.7. Atomic force microscopy

Tapping mode AFM images were obtained using a Multi-Mode SPM with Nanoscope IIIa controller (Digital Instruments, Santa Barbara, CA). Nanosensors silicon probes (type NCH) distributed by Molecular Imaging (Tempe, AZ) were used for tapping mode AFM in air. The images were scanned at a scan rate of 1 Hz on an E-type scanner. A resolution of 512 pixels/line was used for all AFM images. Flattening algorithms in the Nanoscope software were used to reduce vertical scanner drift, image bowing, skips, and any other artifacts that may have resulted in vertical offsets during scanning.

2.8. Fluorescence experiments

Fluorescence images were taken with a Nikon Eclipse E800 epifluorescent microscope equipped with a high-pressure mercury arc lamp source. All images were obtained using a 20× objective. A high-resolution Photometrics CoolSNAP HQ CCD camera (Roper Industries Inc., Duluth, GA) was used to capture the images, and Metamorph software (Universal Imaging Corp., Downington, PA) was used to collect and analyze the images. For imaging, the bilayer was assembled into a sandwich with another glass cover slip and placed in a sample holder designed to keep the bilayer hydrated. All imaging was conducted at room temperature, ~20 °C. The diffusion coefficient was determined using fluorescence recovery after photobleaching (FRAP) and analyzed by the Axelrod method assuming a circular disc beam spot [45]. The samples were photobleached by contracting the field diaphragm (~160 pixel diameter). The region was photobleached for ~30 s and subsequently imaged with an exposure time of 10–50 ms to monitor the recovery. The measured fluorescence intensity of the photobleaching region was plotted versus time. The intensity data was fit to a single exponential decay to determine the fluorescence intensity at infinite time, $F(\infty)$. From this recovery curve, the time at which the fluorescence intensity has recovered to half of $F(\infty)$, $\tau_{1/2}$, was determined in order to calculate the fluorophore diffusion constant, D:

$$D = 0.22\frac{w^2}{\tau_{1/2}} \quad (1)$$

where w is the photobleaching spot diameter.

3. Results

3.1. Monolayer properties at the air–water interface

Fig. 3 shows surface pressure–area isotherms of the CO15/egg-PC mixed monolayers at the air–water interface for different molar concentrations of copolymer: 0, 5, 60, and 100 mol% CO15. As discussed in Section 2, the mol% refers

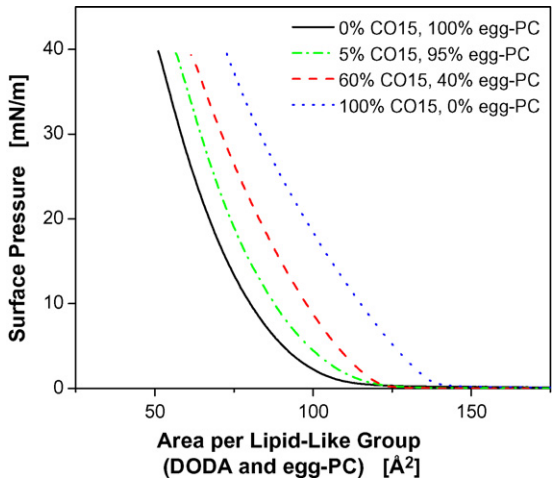

Fig. 3. Langmuir isotherms of CO15 and egg-PC mixed monolayers at $T = 26\,^{\circ}C$.

to the lipid-like DODA moieties on the copolymer because each CO15 has multiple DODA functionalities. Thus, Fig. 3 represents the relationship between the monolayer film pressure and the area per lipid-like group (both DODA and egg-PC). The isotherm for 0 mol% CO15 monolayer (pure egg-PC) is similar to what has been previously reported [46,47]. As the percentage of CO15 increases, the mean molecular area also increases indicating that the copolymer DODA groups occupy more space than the egg-PC lipids. All of the isotherms have a similar shape indicating that, even in the case for 100 mol% CO15, the interactions of the alkyl chains at the air–water interface dominate the film behavior. The isothermal behavior typically seen for lipopolymers with significant polymer interaction in the subphase is not seen here [48–50]. At high surface pressures, the slopes of the isotherms are nearly identical for all mixtures. However, at very low surface pressures, there is a sharp rise in the surface pressure for the 60 and 100 mol% CO15 monolayers, whereas the surface pressure increases more gradually and shows no distinct transitions for the 0 and 5 mol% CO15 monolayers. This suggests that the monolayers with higher percentage mixtures of CO15 bypass any expanded state and immediately go to a state of higher organization. This can be examined more quantitatively by comparing the monolayer compressibilities. The compressibility, C, is defined as:

$$C = -\frac{1}{a}\left(\frac{da}{d\pi}\right) \quad (2)$$

where a is the mean molecular area and π is the surface pressure. Table 1 summarizes the compressibility data for the mixed monolayers. As qualitatively described above, the compressibilities of the monolayers are nearly identical at $\pi = 38$ mN/m. However, the compressibilities of the monolayer at $\pi = 1.5$ mN/m decrease significantly with increasing molar percentage of CO15 indicating that, even at this low surface pressure, the molecules in the higher percentage CO15 films are in a state of increased organization.

Another parameter used to characterize monolayers at the air–water interface is the "limiting area". The limiting area can be obtained by extrapolating the steep, high pressure linear

Table 1
Compressibilities and limiting areas of CO15/egg-PC mixed monolayers

	C (π = 1.5 mN/m)	C (π = 38 mN/m)	Limiting area (Å^2/molecule)
0% CO15	0.058	0.013	79
5% CO15	0.053	0.013	88
60% CO15	0.029	0.017	104
100% CO15	0.025	0.016	118
DODA	–	–	23.1[a]

[a] For DODA at T = 28 °C [51,52].

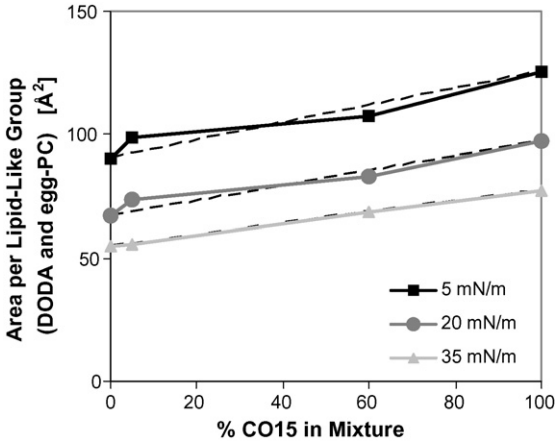

Fig. 4. Monolayer miscibility for CO15/egg-PC. The mean molecular area of the mixed monolayer is shown as a function of percentage of CO15 in the mixture for three different surface pressures. The dotted lines represent ideal mixing.

portion of the isotherm back to the x-axis (π = 0 mN/m). This "area at zero-pressure" can be thought of as the mean molecular area in a hypothetical state of uncompressed close-packed configuration. The limiting areas are shown in Table 1. The limiting area of DODA obtained from literature is also shown. (Note that the temperature at which this limiting area was determined is slightly higher at 28 °C. The limiting area at 26 °C will likely be slightly smaller than 23.1 Å^2.) In an ideal mixture, if the mixed monolayers were composed of individual DODA molecules mixed with egg-PC molecules, the limiting area of the mixtures would decrease with increasing DODA since the limiting area of DODA is much smaller than egg-PC. Instead, the opposite trend is seen. The limiting area is found to increase with increasing CO15, indicating that the polymer backbone influences the monolayer behavior. However, another important factor that influences the limiting area of the monolayer is the miscibility of the components. For an ideal two-component system:

$$a_{12} = x_1 a_1 + x_2 a_2 \quad (3)$$

where a_{12} is the mean molecular area in the two-component mixed film at a given surface pressure, x_1 and x_2 the mole fractions of each component, and a_1 and a_2 are the mean molecular areas in the two pure component films at the same surface pressure. Thus, for an ideal mixture in which the components do not interact with each other, the plot of a_{12} versus x_1 should be a straight line. Any deviation from this straight line suggests non-ideal mixing interactions between the two components. Fig. 4 plots the average area of the mixed monolayer (a_{12}) versus the percentage of CO15 component (x_1). The dotted lines show the case for ideal mixing. At 35 mN/m, the mean molecular area for the mixture essentially follows the ideal case. At the lower surface pressures of 5 and 20 mN/m, there is only a slight positive deviation at 5 mol% CO15 and a slight negative deviation at 60 mol% CO15. These results suggest that the CO15/egg-PC interactions are not significantly different than the egg-PC/egg-PC and CO15/CO15 interactions.

As discussed above, the isothermal behavior of the monolayers was relatively similar for all mixtures. However, the 5 mol% CO15 monolayer was chosen for further experiments because the intended application of this model membrane is as a platform capable of housing membrane proteins. The 60 and 100 mol% CO15 monolayers may present a less favorable environment for incorporating proteins due to the majority of the lipids in the proximal leaflet being pinned to the substrate. However, it should be noted that this ratio of CO15 to egg-PC could be tailored for the specific protein of interest. As a general approach, we have continued with the 5 mol% CO15 mixture.

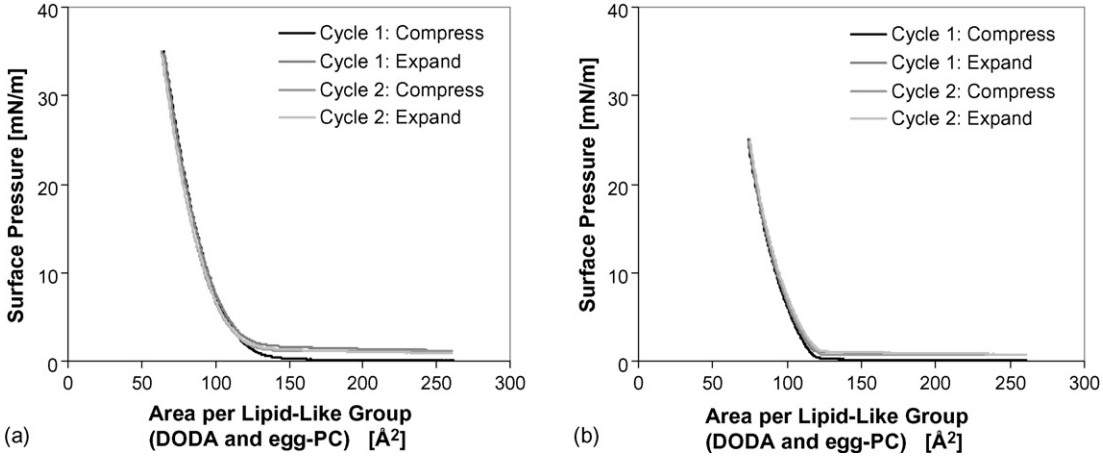

Fig. 5. Compression and expansion cycles of 5 mol% CO15 up to: (a) 35 mN/m and (b) 25 mN/m.

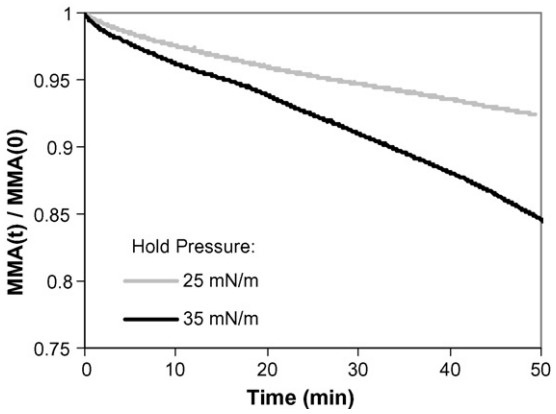

Fig. 6. Isobaric creep test of 5 mol% CO15 at two surface pressures.

Hysteresis experiments were conducted to determine whether molecular interactions that occur in the monolayer during compression are reversible or irreversible. Fig. 5 shows two compression and expansion cycles for 5 mol% CO15 with an upper surface pressure limit of 35 mN/m (Fig. 5a) or 25 mN/m (Fig. 5b). Both figures show that the isotherm is reversible indicating that no states are being formed due to cohesive interactions. This is expected as the isotherm shown in Fig. 3 did not indicate any distinct transitions.

An isobaric creep test was conducted for the 5 mol% CO15 monolayer at two surface pressures: 25 and 35 mN/m (Fig. 6). The monolayer appears to be significantly more stable at the lower surface pressure. After 50 min of holding at the target surface pressure, the monolayer at 35 mN/m had decreased in mean molecular area by 15% while the monolayer at 25 mN/m had decreased by only 8%. Although the monolayer at 35 mN/m is in a state of higher order than at 25 mN/m, it is also less compressible than at 25 mN/m. This higher instability in the monolayer could lead to buckling of the monolayer or loss of material at the interface due to the high surface pressure.

3.2. Langmuir–Blodgett transferred monolayers

The CO15/egg-PC mixed monolayers were transferred to solid substrates via LB transfer once they had been compressed to a suitable state of organization. Because the stability of the film at the air–water interface may directly influence the quality of the film transferred to the substrate, the results of the isobaric creep tests were used to select a transfer pressure of 25 mN/m. Tapping-mode AFM was used to confirm this choice of surface pressure by observing the quality and homogeneity of various transferred films. AFM images of the 5 mol% CO15 monolayer transferred at 25 and 38 mN/m and the 20 mol% CO15 monolayer transferred at 38 mN/m are shown in Fig. 7. Also shown is the mean roughness, R_a, of each film. Although both of the 5 mol% CO15 films appear to be relatively homogeneous, the 20 mol% CO15 film transferred at 38 mN/m is very heterogeneous with many irregularities. The size of the irregularities is widely distributed, with the tallest features reaching 4 nm. Because the state of the monolayer likely influences the state of the bilayer, a transfer pressure of 25 mN/m was used for bilayer experiments.

Table 2
Diffusion coefficients for 5% CO15, 95% egg-PC tethered lipid bilayers

	Diffusion coefficient ($\mu m^2/s$)
Distal leaflet	0.6 ± 0.3
Proximal leaflet	0.6 ± 0.2
Solid-supported lipid bilayer	1.4 ± 0.5

3.3. Bilayers

The monolayer film containing 5 mol% CO15 was transferred to the substrate at 25 mN/m. After the photochemical reaction in which the copolymer is covalently attached to the substrate, egg-PC vesicles labeled with Texas Red-PE were fused to the monolayer to deposit the distal leaflet of the bilayer. This bilayer assembly was then imaged directly using fluorescence microscopy. Images of the final completed bilayer are shown in Fig. 8. As shown in Fig. 8a, the bilayer appears homogeneous, but there are a few scattered bright spots that may simply be adsorbed vesicles that were not fully removed during the rinsing process after vesicle fusion.

The fluidity of the bilayer can also be important for many model membrane applications. Thus, the fluidity of the bilayer was measured using fluorescence recovery after photobleaching (FRAP) experiments. Images taken during the FRAP experiments are shown in Fig. 8b and c. The calculated diffusion coefficient of the Texas Red-PE probe in the distal leaflet is shown in Table 2. In addition, the proximal leaflet was labeled with Texas Red-PE to permit measurement of the diffusion coefficient of the

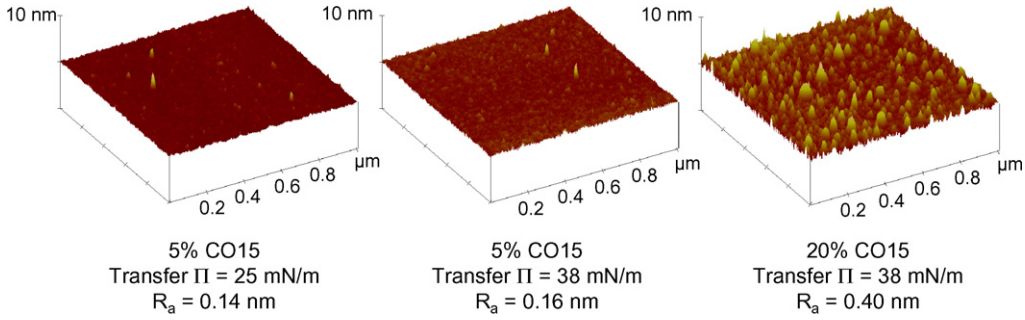

Fig. 7. Tapping-mode AFM images of transferred CO15 monolayers. The scan size is 1 μm × 1 μm.

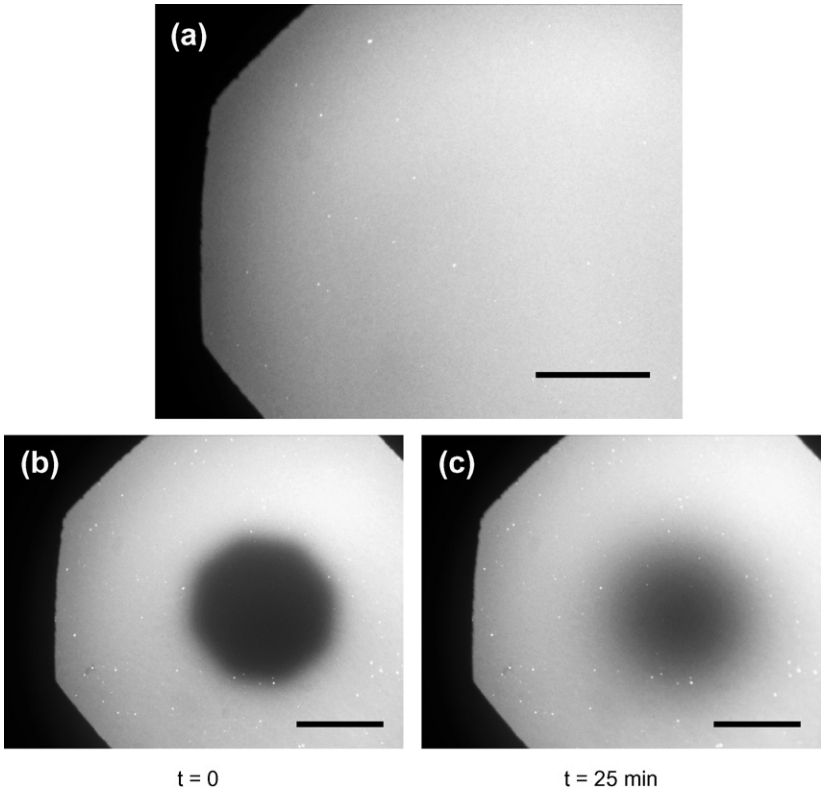

Fig. 8. Fluorescence images of 5 mol% CO15 bilayer. The monolayer was transferred at a transfer pressure of 25 mN/m and at a transfer speed of 0.5 mm/min. Egg-PC vesicles doped with 1% Texas Red-PE were used to deposit the distal leaflet of the bilayer. Image (a) shows the homogeneous bilayer. Images (b) and (c) were taken during the FRAP recovery sequence. The scale bar in each image represents 100 μm.

proximal leaflet. (Note that the vesicles used to deposit the distal leaflet for this sample were not labeled with Texas Red-PE). A reference diffusion coefficient of a solid-supported lipid bilayer formed directly on glass using vesicle fusion is also shown. The diffusion coefficients of the two leaflets are both 0.6 $\mu m^2/s$, roughly half of that of the solid-supported lipid bilayer.

4. Discussion

We have developed a random copolymer-tethered lipid bilayer system in which an understanding of the monolayer properties and lipopolymer design was used to produce a continuous, fluid bilayer on a well-defined platform. Based on the surface pressure–area isotherms of the mixed CO15/egg-PC monolayers, we found that the alkyl chain interactions of the DODA and egg-PC tails dominated the monolayer behavior. However, the isotherms shifted to greater mean molecular area with increasing CO15 (despite the relatively small limiting area of the DODA molecule), and the miscibility data indicated that interactions between the CO15 DODA and egg-PC molecules did not deviate significantly from ideal. These data suggest that the presence of the glyco-monomers was affecting the monolayer by expanding the interactions beyond what would be the case for individual DODA molecules but not to the extent that typical lipopolymer conformational behavior such as pancake-mushroom-brush transitions was seen in the isotherms. For this random CO15 copolymer there is one DODA-monomer for approximately six glyco-monomers on average. Although six glyco-monomers are not enough monomers to exhibit random walk behavior (see Fig. 9), water is a good solvent for the glyco-monomers, and this may lead to the expanded isotherm with increased CO15.

One concern for these tethered lipid bilayer systems is that the tethered lipid molecules may segregate from the free lipids, leading to macroscopic domains within the proximal leaflet. The hysteresis experiments on the 5 mol% CO15 monolayer indicated that the monolayer behavior was completely reversible up to 35 mN/m. Although this does not eliminate the possibility of phase separation within the monolayer, it does preclude the formation of irreversible condensed states.

The optimum conditions for forming a continuous and fluid bilayer were pursued, and the lateral diffusion within both lipid leaflets was measured. Merkel et al. [7] showed that the properties of the individual leaflets of the bilayer influence the fluidity

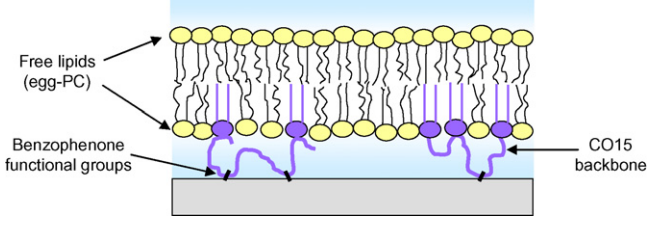

Fig. 9. Schematic representation of CO15-tethered lipid bilayer.

of the opposing leaflet. Thus, a transfer pressure of 25 mN/m was chosen for the LB transfer of the proximal leaflet based on the monolayer stability (isobaric creep experiments) and homogeneity (AFM experiments). We found that a homogeneous and fluid bilayer could be formed on this monolayer with a diffusion coefficient of 0.6 $\mu m^2/s$ for both leaflets. This is slightly higher than was seen previously in a different copolymer system developed by Shen et al. [39]. They found a distal leaflet diffusion coefficient of 0.1 $\mu m^2/s$ for a poly(ethyloxazoline-*co*-ethyleneimine) based system at roughly the same tethering density. However, this system used 1,2-dimyristoyl-*sn*-glycero-3-phosphocholine (DMPC) as the free lipid in the proximal leaflet, which has a phase transition temperature of 23 °C (very close to the imaging conditions of room temperature). Thus, it is difficult to discern whether the difference in polymer chemistry or the coupling of the distal leaflet lipids to a potentially rigidified proximal leaflet resulted in the lower diffusion coefficient. The diffusion coefficient measured in the distal leaflet was less than half of the diffusion coefficient seen in a solid-supported lipid bilayer. Note that the DODA groups in the proximal leaflets are either immobile or have very limited short-range mobility since they are attached to the CO15, which is bound to the substrate. It is likely that these static points decrease the mobility of the lipids in the distal leaflet via frictional coupling. For example, Wagner and Tamm [36] observed similar behavior for their telechelic poly(ethylene glycol) based system. They found that the diffusion coefficient in the distal leaflet for their tethered system decreased from 1.32 to 0.89 $\mu m^2/s$ as tethering was increased from 0 to 10%. Naumann et al. [38] also saw a decrease in distal leaflet lipid diffusion coefficient with tethering density for their telechelic poly(ethyloxazoline) based system. Although they found much higher diffusion coefficients (17.7 $\mu m^2/s$ for 5% tethering and 9.7 $\mu m^2/s$ for 10% tethering), this similar trend of decreasing distal leaflet diffusion with proximal leaflet tethering was measured.

Reports on the proximal leaflet diffusion have been conflicting. In our copolymer system, a decrease in proximal leaflet diffusion with increased tethering density was observed. Naumann and coworkers [53] also found that the proximal leaflet diffusion decreased linearly with increasing tethering density. They described this behavior using a percolation model. In contrast, Wagner and Tamm [36] found that the diffusion coefficient stayed relatively constant between 0 and 10 mol% tethering. However, it is difficult to make direct comparisons with these reported systems as the proximal leaflet lipids exist in a significantly different environment for each system. The poly(ethylene glycol) and poly(ethyloxazoline) systems both used telechelic lipopolymers in contrast to our copolymer system that has approximately one DODA-monomer for every six glyco-monomers. In addition, all of these systems used an aqueous subphase, but the swelling behavior will differ due to individual polymer interactions with the subphase. Our observed decrease in proximal diffusion may be caused by obstructed diffusion from the immobile DODA barriers. In addition, the proximal leaflet may experience slightly increased viscous molecular friction due to the short copolymer segments between DODA groups, which are tethered to the surface. However, the fluidity demonstrated in this copolymer-tethered lipid bilayer is likely to be sufficient for many protein applications.

It is important to remember that this random copolymer-tethered lipid bilayer is not targeted for applications requiring a large separation distance. As the CO15 copolymer has an average of one DODA-monomer per six glyco-monomers, a conservative estimate of the average distance between DODA-monomers (using an ideal C–C bond distance of 1.26 Å) is 1.5 nm. This would not provide a substantial increase in separation distance between the bilayer and substrate as depicted in Fig. 9. Shen et al. [39] found a maximum separation distance of 3 nm for their copolymer system, only slightly greater than the 1–2 nm separation distances of solid-supported lipid bilayers. However, with this random copolymer-tethered lipid bilayer, we have created a bilayer system that maintains bilayer homogeneity and fluidity while potentially enhancing the stability and robustness with the copolymer lipid analogue tethers.

5. Conclusions

We have demonstrated the successful assembly of a random copolymer-tethered lipid bilayer that is homogeneous and fluid. The carefully controlled monolayer of copolymer and free lipids oriented at the air–water interface was transferred onto the silica substrates. AFM images confirmed that the monolayer state chosen for the transfer was smooth and homogeneous. Finally, the distal leaflet was successfully incorporated via vesicle fusion with small unilamellar vesicles. We have studied one of the major biological properties of membranes: the long-range lateral fluidity. Both leaflets of the copolymer-tethered lipid bilayer yielded diffusion coefficients of 0.6 $\mu m^2/s$. Further work needs to be done to look at the effect of tethering concentration on fluidity beyond the 5 mol% CO15 mixture used in the majority of these studies. However, this approach of using a hydrophilic, glyco-acrylate copolymer tethered between the bilayer and substrate is a feasible system for mimicking biological membranes in applications that require added stability and robustness.

Acknowledgments

Financial support was provided by the NSF-MRSEC Program through the Center on Polymer Interfaces and Macromolecular Assemblies (Grant NSF-DMR 9808677) and the NASA HEDS Program (Grant NAG8-1843).

References

[1] E. Sackmann, Science 271 (1996) 43–48.
[2] L.K. Tamm, H.M. McConnell, Biophys. J. 47 (1985) 105–113.
[3] P. Wenzl, M. Fringeli, J. Goette, U.P. Fringeli, Langmuir 10 (1994) 4253–4264.
[4] J. Radler, H. Strey, E. Sackmann, Langmuir 11 (1995) 4539–4548.
[5] C.A. Helm, J.N. Israelachvili, P.M. McGuiggan, Science 246 (1989) 919–922.
[6] P.S. Cremer, S.G. Boxer, J. Phys. Chem. B 103 (1999) 2554–2559.
[7] R. Merkel, E. Sackmann, E. Evans, J. Phys. 50 (1989) 1535–1555.
[8] I.G. Krishnamoorthy, Biochim. Biophys. Acta 1414 (1998) 255–259.
[9] M. Stelzle, G. Weissmuller, E. Sackmann, J. Phys. Chem. 97 (1993) 2974–2981.

[10] G. Wiegand, N. Arribas-Layton, H. Hillebrandt, E. Sackmann, P. Wagner, J. Phys. Chem. B 106 (2002) 4245–4254.
[11] A.A. Brian, H.M. McConnell, Proc. Natl. Acad. Sci. U.S.A. 81 (1984) 6159–6163.
[12] A. Grakoui, S.K. Bromley, C. Sumen, M.M. Davis, A.S. Shaw, P.M. Allen, M.L. Dustin, Science 285 (1999) 221–227.
[13] T.H. Watts, H.E. Gaub, H.M. McConnell, Nature 320 (1986) 179–181.
[14] C.A. Helm, W. Knoll, J.N. Israelachvili, Proc. Natl. Acad. Sci. U.S.A. 88 (1991) 8169–8173.
[15] S. Heyse, T. Stora, E. Schmid, J.H. Lakey, H. Vogel, Biochim. Biophys. Acta 1376 (1998) 319–338.
[16] A. Loidl-Stahlhofen, S. Kaufmann, T. Braunschweig, T.M. Bayerl, Nat. Biotechnol. 14 (1996) 999–1002.
[17] M. Uto, M. Araki, T. Taniguchi, S. Hoshi, S. Inoue, Anal. Sci. 10 (1994) 943–946.
[18] A. Van Oudenaarden, S.G. Boxer, Science 285 (1999) 1046–1048.
[19] T.M. Bayerl, M. Bloom, Biophys. J. 58 (1990) 357–362.
[20] S.J. Johnson, T.M. Bayerl, D.C. McDermott, G.W. Adam, A.R. Rennie, R.K. Thomas, E. Sackmann, Biophys. J. 59 (1991) 289–294.
[21] B.W. Koenig, S. Krueger, W.J. Orts, C.F. Majkrzak, N.F. Berk, J.V. Silverton, K. Gawrisch, Langmuir 12 (1996) 1343–1350.
[22] L.K. Tamm, Biochemistry 27 (1988) 1450–1457.
[23] E. Kalb, S. Frey, L.K. Tamm, Biochim. Biophys. Acta 1103 (1992) 307–316.
[24] M. Stelzle, R. Miehlich, E. Sackmann, Biophys. J. 63 (1992) 1346–1354.
[25] P.Y. Chan, M.B. Lawrence, M.L. Dustin, L.M. Ferguson, D.E. Golan, T.A. Springer, J. Cell Biol. 115 (1991) 245–255.
[26] J. Salafsky, J.T. Groves, S.G. Boxer, Biochemistry 35 (1996) 14773–14781.
[27] G.B. Luo, T.T. Liu, X.S. Zhao, Y.Y. Huang, C.H. Huang, W.X. Cao, Langmuir 17 (2001) 4074–4080.
[28] J. Majewski, J.Y. Wong, C.K. Park, M. Seitz, J.N. Israelachvili, G.S. Smith, Biophys. J. 75 (1998) 2352–2362.
[29] J.Y. Wong, J. Majewski, M. Seitz, C.K. Park, J.N. Israelachvili, G.S. Smith, Biophys. J. 77 (1999) 1445–1457.
[30] J.Y. Wong, C.K. Park, M. Seitz, J. Israelachvili, Biophys. J. 77 (1999) 1458–1468.
[31] G. Elender, E. Sackmann, J. Phys. II 4 (1994) 455–479.
[32] E. Sackmann, M. Tanaka, Trends Biotechnol. 18 (2000) 58–64.
[33] L. Haussling, W. Knoll, H. Ringsdorf, F.J. Schmitt, J.L. Yang, Makromol. Chem. Macromol. Symp. 46 (1991) 145–155.
[34] J. Spinke, J. Yang, H. Wolf, M. Liley, H. Ringsdorf, W. Knoll, Biophys. J. 63 (1992) 1667–1671.
[35] J.C. Munro, C.W. Frank, Langmuir 20 (2004) 10567–10575.
[36] M.L. Wagner, L.K. Tamm, Biophys. J. 79 (2000) 1400–1414.
[37] O. Purrucker, A. Fortig, R. Jordan, M. Tanaka, Chem. Phys. Chem. 5 (2004) 327–335.
[38] C.A. Naumann, O. Prucker, T. Lehmann, J. Ruhe, W. Knoll, C.W. Frank, Biomacromolecules 3 (2002) 27–35.
[39] W.W. Shen, S.G. Boxer, W. Knoll, C.W. Frank, Biomacromolecules 2 (2001) 70–79.
[40] H. Gotz, E. Harth, S.M. Schiller, C.W. Frank, W. Knoll, C.J. Hawker, J. Polym. Sci. Part A 40 (2002) 3379–3391.
[41] G. Dorman, G.D. Prestwich, Biochemistry 33 (1994) 5661–5673.
[42] O. Prucker, C.A. Naumann, J. Rühe, W. Knoll, C.W. Frank, J. Am. Chem. Soc. 121 (1999) 8766–8770.
[43] L.D. Mayer, M.J. Hope, P.R. Cullis, Biochim. Biophys. Acta 858 (1986) 161–168.
[44] R.C. MacDonald, R.I. MacDonald, B.P.M. Menco, K. Takeshita, N.K. Subbarao, L.R. Hu, Biochim. Biophys. Acta 1061 (1991) 297–303.
[45] D. Axelrod, D.E. Koppel, J. Schlessinger, E. Elson, W.W. Webb, Biophys. J. 16 (1976) 1055–1069.
[46] A.B. Serfis, S. Brancato, S.J. Fliesler, Biochim. Biophys. Acta 1511 (2001) 341–348.
[47] Q. Fan, A. Relini, D. Cassinadri, A. Gambacorta, A. Gliozzi, Biochim. Biophys. Acta 1240 (1995) 83–88.
[48] C.A. Naumann, W. Knoll, C.W. Frank, Biomacromolecules 2 (2001) 1097–1103.
[49] C.A. Naumann, C.F. Brooks, W. Wiyatno, W. Knoll, G.G. Fuller, C.W. Frank, Macromolecules 34 (2001) 3024–3032.
[50] C.A. Naumann, C.F. Brooks, G.G. Fuller, T. Lehmann, J. Ruhe, W. Knoll, P. Kuhn, O. Nuyken, C.W. Frank, Langmuir 17 (2001) 2801–2806.
[51] H. Gotz, K. C. Weng, W. W. Shen, C. J. Hawker, W. Knoll, C. W. Frank, in preparation.
[52] W. W. Shen, Ph.D. thesis, Stanford University, Stanford, CA, 2002.
[53] M.A. Deverall, E. Gindl, E.K. Sinner, H. Besir, J. Ruehe, M.J. Saxton, C.A. Naumann, Biophys. J. 88 (2005) 1875–1886.